Predicting the Weather by Watching Aeroplanes: Applying Refractive Techniques to Air-plane ADSB Radio Wave Signals in the Lower Troposphere for Determining Relative Humidities.

Matthew Evans

27th March 2019

Abstract

Various wave properties were investigated by exploring water waves in a ripple tank and studying the diffraction of laser light. A value of 0.18 ± 0.05 ms^{-1} for water wave speed at varying frequencies and a fixed depth of $h = 1.0 \pm 0.3$ cm was obtained and the one generated by using $v \approx \sqrt{gh}$ [4] was 0.3 ± 0.1 ms^{-1}. The angles of incidence and reflection for the reflection of water waves at a barrier were found to be $41 \pm 2^{\circ}$ and $41 \pm 2^{\circ}$ respectively. The water wave speed was also investigated at a fixed frequency of 20 Hz with varying depths allowing a value of 4.4 ± 0.1 ms^{-2} for the acceleration due to gravity to be determined with the known value as 9.8 ms^{-2}. The value for the wave speed at varying frequencies was different to the one expected lying outside the uncertainty range, also the value of g was different to the known value however, the angle of incidence and reflection were shown to be equal to each other. Experimental values determined for the wavelength of the laser light source for the single and double-slit configurations was found to be 652.1 ± 0.7 nm and 655.71 ± 0.03 nm respectively, using a 0.3mm aperture, a slit width of $a = 0.04$ mm and slit separation of $d = 0.5$ mm: the value of the device is 650 ± 10 nm [8]. These values compare well with the device value along with other single and double-slit configurations generating wavelengths that compared well with the device value but, all the uncertainties of the experimental values of the wavelength were underestimated. By understanding water waves and electromagnetic waves, hydroelectric power and chemical spectra analysis could be optimised for the benefit of many modern day appliances.

Contents

1 Introduction

The Earth's weather in the troposphere is a complicated dynamical system with many factors playing a crucial role in its development. Four of the most important are temperature, pressure, wind velocity and humidity. During this project, the relative humidity (RH) of the troposphere was investigated by treating it as constant (homogeneous) in order to obtain a relative humidity values. By obtaining values for the relative humidity many benefits can be obtained. One benefit might be that by knowing the relative humidity this could be used in our day-to-day lives to gain an idea of what the weather will be on a particular day, another is that this could give more accurate rainfall patterns allowing farmers to optimise weather conditions when planting crops. Furthermore, the prediction of heavy rainfall could be predicated — saving lives in the case of serious flooding. Thus, the relative humidity of the troposphere is of crucial interest to weather forecasters and this project was carried out in association with the Met Office to help develop their forecasting techniques.

At present, this is difficult to measure directly and only a small number of aircraft have such devices, for example Aircraft Meteorological Data Relay (AMDAR), on board [1] and these are often expensive which limits further opportunities using this method of measurement. An alternative approach in measuring humidity which has been proposed [1] is to use Automatic Dependent Surveillance Broadcast (ADSB) signals from air planes where many of these aircraft have this equipment on board. Therefore, these broadcasts containing aircraft information such as position, velocity, altitude and so on, can be continually obtained by ground monitoring facilities from many different aircraft. By studying how ADSB radio wave signals are refracted within the Earth's lower atmosphere, this could provide a way of obtaining the water vapour distribution thus give relative humidity values.

2 Theory

The speed of waves, v, can be determined by using

$$v = \lambda f \tag{1}$$

where λ is the wavelength and f is the frequency of the waves - the number of waves that pass a given point per second. However, the speed of mechanical waves often depend upon the medium which they travel, in addition to many other factors. For water waves, the speed depends on depth. For shallow depths, this is given by [4]

$$v \approx \sqrt{gh} \tag{2}$$

where g is the acceleration due to gravity and h is the measured depth of the water used in the ripple tank. For the interested reader, a more detailed analysis of water waves can be found at [4].

When a wave front approaches at an angle to a boundary reflection occurs. This is when the angle of incidence, θ_i is equal to the angle of reflection, θ_r at the boundary

$$\theta_i = \theta_r \tag{3}$$

$$I = I_0 \frac{sin^2\alpha}{\alpha^2} \tag{4}$$

where $\alpha = (\pi a sin\theta)/\lambda$, λ is the wavelength of the light and a is the slit width.

For two slits, the intensity of diffracted light into an angle θ [2] is

$$I = I_0 \frac{sin^2\alpha}{\alpha^2} cos^2\delta \tag{5}$$

where $\delta = (\pi d sin\theta)/\lambda$ and d is the separation distance between the two slits. A derivation for equations (4) and (5) involving a geometrical approach and phasor diagrams can be found from [3]. These equations can also be dervied by considering Fourier transforms and the convolution theorem and approach using these techniques can be found from [7].

For the experimental configuration that was considered, the small angle approximation could be used. Therefore the single slit intensity equation (4) can be re-expressed as

$$I \approx I_0 \frac{sin^2 \frac{\pi a x}{L\lambda}}{\left(\frac{\pi a x}{L\lambda}\right)^2} \tag{6}$$

where the intensities are normalised so, $I_0 = 1$ and L is the slit to screen separation distance and x is the screen position ($L >> x$).

Similarly, the double slit intensity equation (5) can be re-expressed due to to the small angle approximation

$$I \approx I_0 \frac{sin^2 \frac{\pi a x}{L\lambda}}{\left(\frac{\pi a x}{L\lambda}\right)^2} cos^2 \frac{\pi d x}{L\lambda} \tag{7}$$

where again the intensities are normalised in the experiments so $I_0 = 1$ and all the other symbols have their usual meaning with $L >> x$.

Using equation (4), the intensity minima for a single slit occurs when α is a multiple of π. This therefore means that

$$sin\theta = \frac{m\lambda}{a} \quad , \quad (m = \pm 1, \pm 2, ...) \tag{8}$$

If L'Hôpital's rule [3] is applied to equation (4) in the limit as the intensity at $\alpha \to 0$ is found to be $I = I_0$ as expected. When the detector to slit distance is big, the small angle approximation can be used. Equation (8) can then be approximated to

$$\theta \approx \frac{m\lambda}{a} \quad , \quad (m = \pm 1, \pm 2, ...) \tag{9}$$

The intensity maxima of a single slit diffraction pattern can be approximately found by using equation (4) and realising that they occur when the sine function is a maximum (± 1) [3]. In other words, when

$$\alpha = \pm\left(m + \frac{1}{2}\right)\pi \quad , \quad (m = 0, 1, 2, ...) \tag{10}$$

However, upon further analysis of applying differentiation to equation (4) and setting equal to zero to find the maxima it is found that the there is no maxima at $m = 0$ [3]. Therefore, when equation (10), with $m \neq 0$, is subsituted into equation (4) the intensity maxima, I_m is approximately given by [3]

$$I_m \approx \frac{I_0}{\left(m + \frac{1}{2}\right)^2 \pi^2} \quad , \quad (m = \pm 1, \pm 2, ...) \tag{11}$$

3 Method

3.1 Mechanical Waves

3.2 Electromagnetic Waves

4 Results

Figure 1 shows two plots of radial distance from the centre of the Earth, R against the increment angle measured from the vertical through the centre of the Earth, θ for a given observed angle range of 0.1° - 0.11° for early (Figure 1a) and late (Figure 1b) times of observation on 26$^{\text{nd}}$ August 2019 starting at 11:45 am. Furthermore, Figure 2 and Figure 3 show additional plots of these R and θ positions for different observed angle ranges of 0.3° - 0.31° and 0.5° - 0.51° respectively. Again, the early times of observation are shown for these different observed angles ranges in Figure 2a and Figure 3a at observed angle ranges of 0.3° - 0.31° and 0.5° - 0.51° respectively. Whereas the late times are shown in Figure 2b and Figure 3b for the observed angle ranges of 0.3° - 0.31° and 0.5° - 0.51° respectively. All these plot values are shown for the plane positions, in addition to the model relative humidity curves for 0%, 100% and the best fitting relative humidity curve for the plane positions.

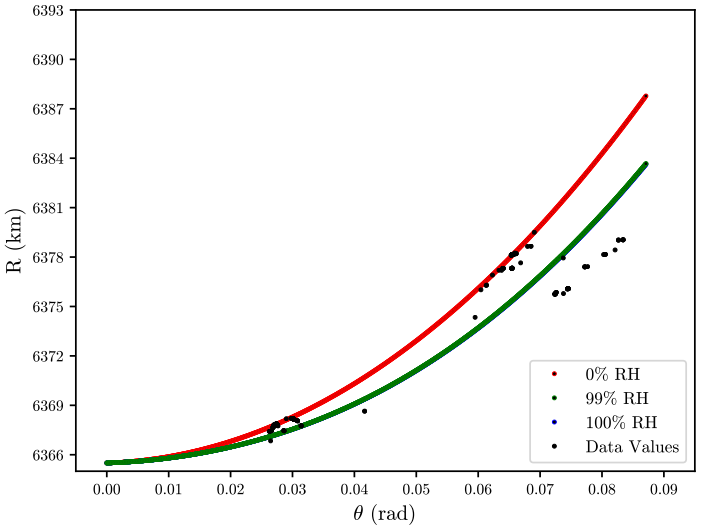

(a) R vs θ for early times (the first 5000s) of observation.

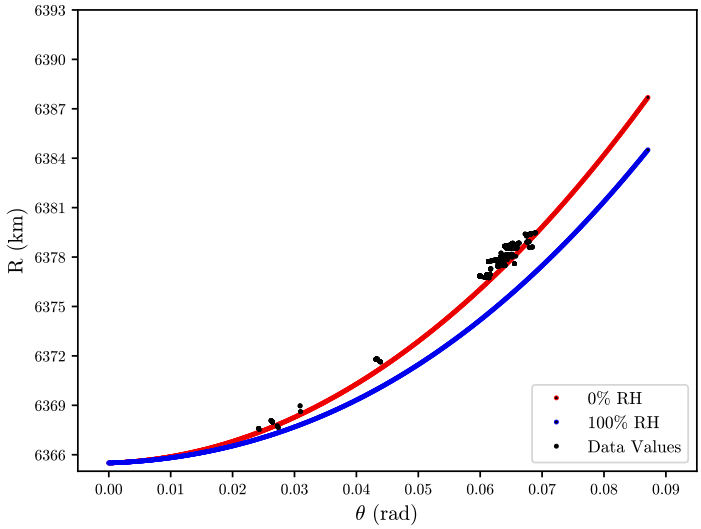

(b) R vs θ for late times (the last 5000s) of observation.

Figure 1: Plots of radial distance, R against increment angle, θ from the vertical through the centre of the Earth for plane positions (shown in black) at a given observed angle range between 0.1° - 0.11° for early and late times of observation.

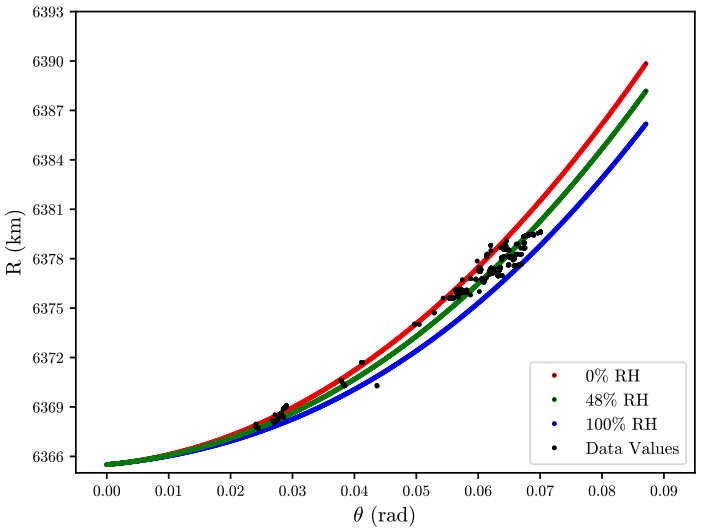

(a) R vs θ for early times (the first 5000s) of observation.

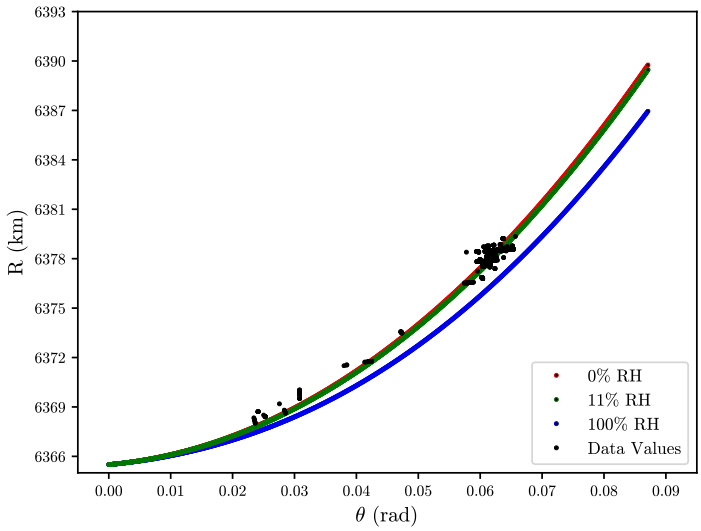

(b) R vs θ for late times (the last 5000s) of observation.

Figure 2: Plots of radial distance, R against increment angle, θ from the vertical through the centre of the Earth for plane positions (shown in black) at a given observed angle range between 0.3° - 0.31° for early and late times of observation.

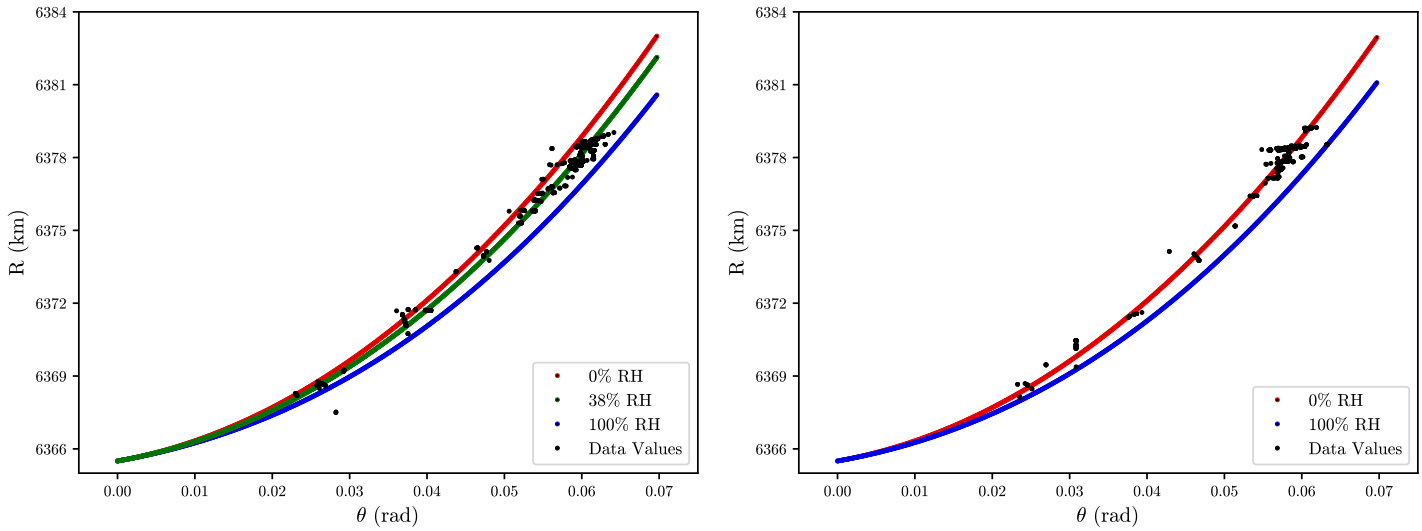

(a) R vs θ for early times (the first 5000s) of observation.

(b) R vs θ for late times (the last 5000s) of observation.

Figure 3: Plots of radial distance, R against increment angle, θ from the vertical through the centre of the Earth for plane positions (shown in black) at a given observed angle range between 0.5° - 0.51° for early and late times of observation.

Table 1 compares the obtained values for the relative humidity from the best fitting (green) curves in Figure 1a, Figure 2a and Figure 3a to the mean of the actual relative humidities obtained from [7] along with their estimated errors for each of the observed angle ranges at early times of observation.

Table 1: A table comparing generated relative humidities (RH) from an interpolative and least squares method for the various different observed angle, ϕ_0 ranges investigated to the mean of the actual RH values given by [7] for the early times of observation (first 5000s).

Observed Angle Range ϕ_0 (°)	Generated RH (%)	Actual RH (%) [7]
0.10 - 0.11	99 ± 8	74 ± 4
0.30 - 0.31	48 ± 3	74 ± 4
0.50 - 0.51	38 ± 3	74 ± 4

Table 2 compares the obtained values for the relative humidity from the best fitting (green) curves in Figure 1b, Figure 2b and Figure 3b to the mean of the actual relative humidities obtained from [7] along with their estimated errors for each of the observed angle ranges at late times of observation.

Table 2: A table comparing generated relative humidities (RH) from an interpolative and least squares method for the various different observed angle, ϕ_0 ranges investigated to the mean of the actual RH values given by [7] for the late times of observation (last 5000s).

Observed Angle Range ϕ_0 (°)	Generated RH (%)	Actual RH (%) [7]
0.10 - 0.11	-	77 ± 5
0.30 - 0.31	$11 \pm <1$	77 ± 5
0.50 - 0.51	-	77 ± 5

The errors for the generated relative humidities were estimated in Table 1 and Table 2 by using the error on the mean for the baseline temperature T_b [7], baseline pressure P_b [7] and observed angle ϕ_0. The following were used to obtain these errors

$$\delta T_b = \frac{\sigma(T_b)}{\sqrt{N_{T_b}}} \tag{12}$$

$$\delta P_b = \frac{\sigma(P_b)}{\sqrt{N_{P_b}}} \tag{13}$$

$$\delta\phi_0 = \frac{0.03}{\sqrt{N_{\phi_0}}} \tag{14}$$

where $\sigma(T_b)$, $\sigma(P_B)$ are the standard deviations of the baseline temperature and pressure respectively, 0.03 is the known error in the observed angle as given by internal project communications, N_{T_b}, N_{P_b} and N_{ϕ_0} are the number of baseline temperature, pressure and observed angle readings considered.

These estimated errors given in (14), (**??**) and (**??**) were added to the mean values for the baseline temperature, baseline pressure and observed angle when calculating the refracted ray path using the appropriate computer program. This gave an upper bound on the relative humidity value. Thus, the difference between the upper bound of the relative humidity and the relative humidity generated by using the average of these values gave an estimated error for the generated relative humidity value.

5 Discussion

6 Conclusion

References

[1] Stone E.K and Kitchen M, 2015, Introducing an Approach for Extracting Temperature from Aircraft GNSS, Journal of Atmospherics and Oceanic Technology, Vol 32, pages 736 - 743. and Pressure Altitude Reports in ADS-B Messages

[2] College of Engineering, Mathematics and Physical Sciences, University of Exeter, PHY2026, *Diffraction and Interference Worksheet* (Accessed 8th February 2019).

[3] Young, Hugh D and Freedman, Roger A, *University Physics*, 13th Edition, 2014, Chapter 36, pages 1312 - 1322.

[4] Barber N.F, *Water Waves*, 1st Edition, 1969, Chapter 3, pages 36 - 55.

[5] Pedrotti F.L, Pedrotti S.J, *Introduction to Optics*, (Pearson International Edition) 3rd Edition, 2006, Chapter 11-1: *Diffraction from a Single Slit*, pages 268 - 273.

[6] Pedrotti F.L, Pedrotti S.J, *Introduction to Optics*, (Pears onInternational Edition) 3rd Edition, 2006, Chapter 11-5: *Double-Slit Diffraction*, pages 281 - 284.

[7] Met Office Weather Observations Website, 22nd November 2019, `https://wow.metoffice.gov.uk/`.)

[8] *Red Diode Laser - Basic Optics - OS-8525A*, `https://www.pasco.com/prodCatalog/OS/OS-8525_red-diode-laser-basic-optics/index.cfm?fbclid=IwAR3gzuNSAoumEZpwYZQO6tX3j1nLhTtLYklX5U6V6HHw5xyHKdszO1ID00I` (Accessed 15th March 2019).